Vera C. Rubin Observatory
Systems Engineering

Rubin Baseline Calibration Plan

Parker Fagrelius, Eli Rykoff

SITCOMTN-086

Latest Revision: 2024-02-09

DRAFT

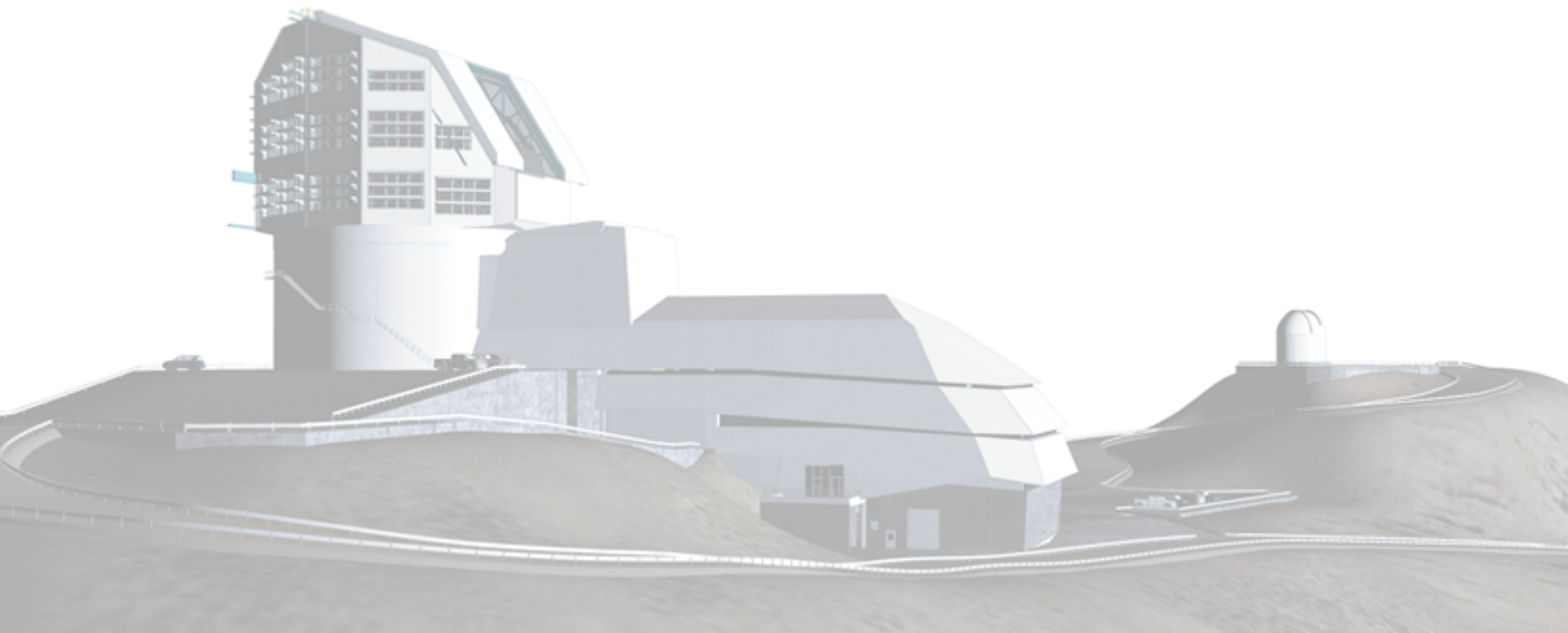

Abstract

Current baseline plan for the year 1 minimum viable product as delivered for ORR.

Change Record

Version	Date	Description	Owner name
1	2023-XX-XX	Unreleased.	Parker Fagrelius

Document source location: `https://github.com/lsst-sitcom/sitcomtn-086`

Contents

Rubin Baseline Calibration Plan

1 Introduction

The basic question of photometric calibration of an astronomical survey is how to take raw counts output from the camera (in arbitrary Analog-Digital Units (ADU)) and convert these to calibrated fluxes in nanoJansky (nJy). In order for this procedure to yield uniform results across the camera and the sky, it must take into account variations that are both achromatic ("gray") and chromatic, that latter of which depend on the spectral energy distribution (SED) of each object. This includes variations in the atmosphere as a function of time and airmass; spatial variations in the filter and detectors; pixel size variations; and various sensor effects such as charge transfer ineffeciency (CTI) and the Brighter Fatter Effect (BFE).

This technote describes the baseline photometric calibration plan for Rubin Commissioning and the first year of data release production for the LSST Survey. This includes plans on performing instrumental signature reduction (ISR), which is also known as "detrending"; correct flat-fielding; background/foreground subtraction; and derivation of a uniform photometric calibration over the full survey. It also includes plans for generating "calibration frames" such as bias, darks, and various types of flats, incorporating LEDs, a class 4 tunable laser, and a novel Collimated Beam Projector (CBP). We expect that this is not the final calibration plan for the LSST survey, but rather a first minimal viable product suitable for the first year of survey observations to meet our required goals for repeatability and uniformity. Further improvements are planned to incorporate more effects, although our plan is to take as much calibration data early on to be able to reprocess early data with improved algorithms.

The calibration plan in this technote is heavily influenced by the Dark Energy Survey, which achieved better than 2 mmag uniformity over 5000 deg^2 in the Southern sky (Rykoff et al. 2023). In particular, we refer the reader to Bernstein et al. 2017 (henceforth B17) and Burke, Rykoff, et al. 2018 (henceforth BR18).

2 Requirements

The requirements on calibration are defined in the Science Requirements Document (LPM-17). The photometric quality and accuracy of the LSST data products is driven by four main

components:

1. Relative photometry (repeatability)
2. Stability across the sky (spatial uniformity)
3. Relative accuracy (color zero-points)
4. Transfer to physical flux scale (external absolute photometry)

The requirements for photometric calibration accuracy are specified using the following error decomposition (valid in the limit of small errors):

$$m_{\mathrm{cat}} = m_{\mathrm{true}} + \sigma + \delta_m(x, y, \theta, \alpha, \delta, \mathrm{SED}, t) + \Delta m \quad (1)$$

where m_{true} is the true magnitude defined by eqs. 4 and 7, m_{cat} is the cataloged LSST magnitude, σ is the random photometric error (including random calibration errors and count extraction errors), and Δm is the overall (constant) offset of the internal survey system from a perfect AB system (the six values of Δm are equal for all the cataloged objects).

Here, δ_m describes the various systematic dependencies of the internal zeropoint error around Δm, such as position in the field of view (x, y), the normalized system response (θ), position on the sky (α,δ), and the source spectral energy distribution(SED). Note that the average of δ_m over the cataloged area is 0 by construction.

The SRD allocates error specifications for the griz bands, with a 50% increase expected for u and y bands. These high level allocations are further broken down to three main elements in Observatory System Specifications (LSE-30). These are Instrument Throughput, Atmospheric Transmittance, and Reference Star Catalogs. The full functional error budget can be found in LSST Document-9553.

where m_{true} is the true magnitude defined by eqs. 4 and 7, m_{cat} is the cataloged LSST magnitude, σ is the random photometric error (including random calibration errors and count extraction errors), and Δm is the overall (constant) offset of the internal survey system from a perfect AB system (the six values of Δm are equal for all the cataloged objects). Here, δ_m describes the various systematic dependencies of the internal zeropoint error around Δm, such as position in the field of view (x, y), the normalized system response (θ), position on the

Design Spec (millimag)	Repeatability	Uniformity	Color Accuracy	External Absolute Photometry
Overall Specification	5	10	5	10
Instrument Throughput	3	2	3	-
Atmospheric Transmittance	3.5	4	3	-
Reference Catalog	2.5	9	3	-

Table 1: TABLE NAME NEEDED

Design Spec (millimag)	Repeatability	Uniformity	Color Accuracy	Abs. Photometry
Overall Specification	5	10	5	10
Instrument Throughput	3	2	3	-
Atmospheric Transmittance	3.5	4	3	-
Reference Catalog	2.5	9	3	-

sky (α, δ), and the source spectral energy distribution (SED). Note that the average of δ_m over the cataloged area is 0 by construction.

The SRD allocates error specifications for the griz bands, with a 50% increase expected for u and y bands. These high level allocations are further broken down to three main elements in Observatory System Specifications (LSE-30). These are Instrument Throughput, Atmospheric Transmittance, and Reference Star Catalogs. The full functional error budget can be found in LSST Document-9553.

From these functional requirements, requirements are allocated to the Telescope & Site (LSE-60) and Data Management (LSE-61) systems to ensure that the functional requirements are met.

3 Instrumental Signature Reduction (ISR)

In this section, we describe the instrument signature removal (ISR) for LSSTCam. After the photons hit the detector surface, there are a number of sensor effects that alter the image as photoelectrons are produced, collected in the detector, clocked and read out, and sent through the amplifier(s) to the analog-to-digital converter (ADC). Each of these steps can imprint an effect, including adding noise, non-linearities, cross-talk, etc. Our goal in ISR is to apply corrections "in reverse" to go from the raw camera output of Analog to Digital Units (ADU) in 16 amplifiers to a "post ISR" image in units of electrons (e^-) that are equiavlent to the

number of photocarriers produced in each pixel incident on the camera. In this stage we do not correct for quantum efficiency as a function of wavelength, as that requires knowledge of each individual source SED. We leave the wavelength dependent effects to the photometric calibration described in Section 4.

3.1 Overscan Correction

The first operation we must perform is "overscan correction" to remove the amplifier bias level. Unfortunately, for many channels the bias level in LSSTCam is not completely stable with time, and thus we support a somewhat complicated overscan subtraction routine, using both serial overscan (the additional readout at the end of each row) and parallel overscan (the additional readout at the end of each column). The software may be configured to use specialized overscan settings on a per-detector and per-amplifier basis.

In our default mode, we first perform row-by-row serial overscan correction to remove the bias level as well as possible bias drift and jumps. We have X overscan pixels per row, and we take the median of each row, skipping the first two columns, using the LSST Science Pipelines integer median sampling algorithm (ref?). This introduces approximately XX ADU of noise, which may or may not be comparable to our read noise (TBD).

For some amplifier channels we need to additionally perform parallel overscan subtraction. One challenge of the parallel overscan subtraction is that hot columns and saturated stars bleed into the parallel overscan region, making these columns unusable for parallel overscan subtraction. In addition, these bright signals inject a crosstalk signal into the other crosstalk regions. Therefore, prior to parallel overscan subtraction we perform crosstalk correction on just the parallel overscan region (see Section 3.4 for details on the crosstalk correction algorithm). Additionally, we mask the regions with saturated parallel overscan and interpolate along the columns. Finally, we perform column-by-column parallel overscan correction.

3.2 Saturation Flagging

After overscan correction, we must flag pixels that are deemed to be "saturated" to ensure that these are handled correctly in the following ISR steps. We have yet to determine which definition of saturation/full-well is appropriate. Possible definitions include (a) the PTC turnoff (where the variance of pixel estimates deviates significantly from Poisson); (b) the level at

which the charge-transfer-inefficiency (see Sec 3.7) cannot be corrected; (c) the maximum possible observed value in a pixel; (d) the level above which the E2V sensors exhibit persistence effects.

3.3 Linearity Correction

The response of the readout system is not completely linear, as the amplification of the voltage in the sense node of the amplifier may not be completely linear. [There are other sources of non-linearity; this seems to be the best place to do this correction, and I would like RHL help in describing these.]

Our linearity correction model is a multi-node spline as original defined by P. Astier (ref?). The linearity correction per amplifier is derived from a series of flat pairs illuminated at different flux levels and contemporaneously monitored with a photodiode. We need to take special care in accounting for the different illumination patterns when the LED is used with different current levels, as well as stray light, and gain variation as a function of temperature (described below).

3.4 Crosstalk Correction

Every time a pixel is clocked out through an amplifier, there is an effect on the voltages in the other amplifiers on the same detector. This crosstalk signal must be corrected by a full matrix for each detector that describes the effect of each "source" amplifier on every "target" amplifier. The crosstalk values for LSSTCam are around XX. Furthermore, there is a non-linearity in the crosstalk response of the LSSTCam amplifiers. These are modeled as a first-order correction to the crosstalk matrix as a function of source signal level (A. Snyder, thesis).

The crosstalk matrix coefficients were derived by A. Snyder using "blobs" projected onto LSSTCam. I do not know how much detail is needed here.

3.5 Bias Subtraction

After correcting for all of these effects, there may be some residual imprint of some bias structure. To generate a bias frame to subtract from the image we take a series of zero-second integrations, perform the above ISR correction steps in order, and take the median.

Note that it is important to perform crosstalk correction prior to bias frame creation to ensure that the crosstalk signal from hot columns is corrected or else these will get imprinted on all of the amplifier segments which is undesirable.

3.6 Gain Normalization

In this step we convert the units of each amplifier from ADU to e^- using the gain measurement. This is a two step process. In the first step, we correct the image to account for the fact that the gain hasa small dependence on readout board (REB) temperature ($\approx 0.06\%/^{\circ}C$), and we must correct for any small temperature shifts to ensure all of our images can use equivalent calibrations. In the second step, we use the gains (e^-/ADU) to convert each amplifier from ADU units to e^- units.

The gain dependence on temperature was estimated via [a method to be TBD] using a dataset [TBD].

After correcting for the temperature shifts, we use the photon transfer curve (PTC) analysis to measure the gain from each amplifier (ref). The PTC analysis was done with XX flat pairs. Details to be described.

3.7 CTI Correction

Now that we have corrected for all the amplifier effects, we can now correct for effects that are in the detector itself. The first of these is charge transfer inefficiency (CTI). As charge is clocked along the serial registers, there is a small amount of charge that may be left behind. In the LSSTCam detectors this is due to charge traps as described in a model from Snyder et al. (ref). The details of the CTI correction algorithm and method of building the CTI correction coefficients is in [ref].

3.8 Variance Plane Creation

We now estimate the variance plane of the image. This is computed by starting with the gain-corrected image itself, assuming Poisson variance. We additionally add in the read noise per amplifier which was estimated from the PTC analysis above.

3.9 Defect Masking and Interpolation

Next we mask all known defects and flag these pixels with the "BAD" mask bit. The defects are determined following the methodology from the camera team (ref?). We have two types of defects, "hot" defects which are determined from looking at high outlier pixels in the combined dark frames, and "cold" defects which are determined from looking at low outlier pixels in the combined flat field frames. Additionally, we mask all pixels in a 7 (?) pixel border around each detector which have very strong lateral electric field distortions at this stage.

After masking, these pixels are interpolated for visual fidelity using an interpolation algorithm that I actually don't know what it is.

3.10 Dark Subtraction

As the exposure is integrating charge, there is some small amount of dark current that accumulates. We determine the dark current by taking a series of 30 second images (to match the survey integration time) and taking a median combination. The typical dark current is small (XX electrons per second) but may be larger for some amplifiers.

3.11 Brighter-Fatter Correction

The Brighter/Fatter effect (BFE) is the result of the fact that as charge accumulates in a pixel it will distort the local electric field and push later arriving photocharges away, with the net result that brighter objects have a slightly broader point spread function (PSF). The BFE kernel is derived from flat field pairs, as this effect will create pixel-to-pixel correlations in the flats. See Broughton et al. for details on our algorithm for estimating the BF kernel as well as correcting it in the pixel images.

3.12 Applying Flat Fields

After the above series of steps, we have an unflattened, gain normalized image with sensor effects removed. See below for some details on flat fielding. I'm not sure how much detail to put here, since the detailed flat discussion is part of the photometric calibration.

4 Photometry with Chromatic Corrections

The fundamental goal of photometric calibration is to estimate the surface brightness of sources across the full sky in a uniform way, as would be measured at the top of the atmosphere (TOA). Our general outline for uniform photometry follows DES and specifically B17 and BR18. Our ground-based telescope will count only a fraction of photons from a celestial source that reaches the top of the Earth's atmosphere after attenuation from the atmosphere, filters, optics, and detector quantum efficiency.

Our overall photometry plan follows BR18, in particular the use of the Forward Global Calibration Method (FGCM). This global calibration algorithm uses repeated observations of stars in multiple bands, through multiple instrumental and atmospheric bandpasses, to simultaneously constrain the atmospheric model as well as standardized TOA star fluxes over a wide range of star colors.

4.1 Chromatic Corrections

For broadband observations through the u, g, r, i, z, y filters, the number of photoelectrons (e^-) produced by a source in a pixel is proportional to the integral of the TOA flux $F_\nu(\lambda)$ (the source spectral energy distribution, or SED) weighted by the observation transmission function, $S_b(x, y, \mathrm{alt}, \mathrm{az}, t, \lambda)$ in a given filter b. We discuss the effect of integrating over the point spread function (PSF) and pixel size variations below.

$$e_b^- = A \int_0^{\Delta T} dt \int_0^\infty F_\nu(\lambda) S_b(x, y, \mathrm{alt}, \mathrm{az}, t, \lambda) \frac{d\lambda}{h_{\mathrm{Pl}} \lambda}, \tag{2}$$

where A is the area of the telescope pupil and ΔT is the duration of the exposure. The position x, y is the location in the focal plane; alt, az are the altitude and azimuth of the observation (the altitude being the more important driver of the variation of the transmission by the atmosphere as a function of airmass). The units of flux $F_\nu(\lambda)$ are erg cm^{-2} s^{-1} Hz^{-1}, and the factor $\frac{d\lambda}{h_{\mathrm{Pl}}\lambda}$ counts the number of photons per unit energy at a given wavelength, where h_{Pl} is Planck's constant.

Following BR18, we definte the "observed passband", which is position- and time-dependent, as such:

$$S_b^{\mathrm{obs}} \equiv S_b(x, y, \mathrm{alt}, \mathrm{az}, t, \lambda). \tag{3}$$

Following Fukugita et al. (1996), we define the AB magnitude of a source to be:

$$m_b^{\rm obs} = -2.5\log_{10}\left(\frac{\int_0^\infty F_\nu(\lambda)\, S_b^{\rm obs}\, \lambda^{-1} d\lambda}{\int_0^\infty F^{\rm AB}\, S_b^{\rm obs}\, \lambda^{-1} d\lambda}\right), \tag{4}$$

where $F^{\rm AB} = 3631\,$Jy. Putting this together with the above equation and simplifying we get:

$$m_b^{\rm obs} = -2.5\log_{10}(e_b^-) + 2.5\log_{10}(\Delta T) + 2.5\log_{10}(\mathcal{I}_0^{\rm obs}) + {\rm ZPT}^{\rm AB}, \tag{5}$$

where

$${\rm ZPT}^{\rm AB} = 2.5\log_{10}\left(\frac{A\, F^{\rm AB}}{h_{\rm Pl}}\right), \tag{6}$$

and Iobs is defined as the integral over the observed passband b:

$$\mathcal{I}_0^{\rm obs}(b) \equiv \int_0^\infty S_b^{\rm obs}(\lambda)\, \lambda^{-1}\, d\lambda. \tag{7}$$

Note that in the formulation so far we are limited by the variety of observed passbands that are encountered in a survey, due to variations in instrument over the focal plane and atmosphere over time. Furthermore, these equations require knowledge of the wavelength dependence of the source SED. Therefore, we define a "standard" magnitude as the broadband magnitude that would be measured if a given source were observed through a standard passband Sstd that we are free to choose:

$$m_b^{\rm std} \equiv -2.5\log_{10}\left(\frac{\int_0^\infty F_\nu(\lambda)\, S_b^{\rm std}\, \lambda^{-1}\, d\lambda}{\int_0^\infty F^{\rm AB}\, S_b^{\rm std}\, \lambda^{-1}\, d\lambda}\right). \tag{8}$$

The difference between this standard magnitude and the observed magnitude is then:

$$\delta_b^{\rm std} \equiv m_b^{\rm std} - m_b^{\rm obs} = 2.5\log_{10}(\mathcal{I}_0^{\rm std}(b)/\mathcal{I}_0^{\rm obs}(b)) + 2.5\log_{10}\left(\frac{\int_0^\infty F_\nu(\lambda)\, S_b^{\rm obs}(\lambda)\, \lambda^{-1}\, d\lambda}{\int_0^\infty F_\nu(\lambda)\, S_b^{\rm std}(\lambda)\, \lambda^{-1}\, d\lambda}\right), \tag{9}$$

where $\mathcal{I}_0^{\rm std}$ is defined as in Eqn. 7.

The decomposition in Eqn. 9 is very useful. First of all, the first term is independent of the

SED, and the SED-dependent "chromatic correction" is entirely in the second term. Second, the chromatic correction term goes to zero if either (a) the source SED is completely flat (as with the reference AB spectrum or (b) the observed passband $S_b^{\rm obs}(b)$ is equal to the standard passband $S_b^{\rm std}(b)$. Therefore, it is important to choose a standard passband as close to the "typical" observing conditions as possible in order to minimize the chromatic corrections, and to ensure that averaging over many observed passbands tends toward the mean (standard) passband. For LSSTCam this is made more challenging by the different shapes of the QE curves of the two types of detectors (E2V and ITL), and so we must decide whether to choose one or the other shape as the standard, or to "split the baby" and choose something in the middle that is representative of neither.

4.2 Observed Passbands

We assume that the instrumental and atmospheric components of the observed passband are independent, and therefore we can decompose $S_b^{\rm obs}$ as such:

$$S_b^{\rm obs}(\lambda) = S_b^{\rm inst}(x, y, t, \lambda)\, S^{\rm atm}({\rm alt}, {\rm az}, t, \lambda), \tag{10}$$

where $S_b^{\rm inst}$ is the instrumental component that depends on location in the detector and focal plane, as well as time and wavelength, and $S_b^{\rm atm}$ is the atmospheric component that depends on pointing in the sky. We address each of the instrumental and atmospheric transmission curves in turn.

4.3 Instrumental Response

We can decompose the instrumental response into different parts that depend on the focal plane and time in different ways. Our initial decomposition is:

$$S_b^{\rm inst}(x, y, t, \lambda) = k_b\, S^{\rm refflat}(x, y, \lambda)\, S^{\rm optics}(t, \lambda)\, S^{\rm CBP}(x, y, \lambda), \tag{11}$$

where $S^{\rm refflat}$ is the "reference flux flat" that normalizes the system response to focused light; $S^{\rm optics}$ describes the change in the opacity of the optical system over time; $S^{\rm CBP}$ is the in-situ chromatic throughput of the system as measured by the collimated beam projector; and k_b is an overall throughput constant at the start of the survey that can be determined with observations of standard stars/white dwarfs.

4.3.1 Change in Opacity of Optical System

We break out the $S^{\text{optics}}(t, \lambda)$ as a separate component, because to first order the dust on the optics and mirror build up smoothly over time, more frequently than we can or want to determine "absolute" calibrated throughput measurements. In the original DES formalism described in BR18 this was only a gray term without wavelength dependence, with offsets determined whenever there was a mirror wash or hardware change. Further experience with DES and Hyper Suprime Cam Special Survey Program (HSC; need ref) demonstrated that the mirror coating degrades chromatically over time due to molecular changes. This chromatic change is visible in all bands, but is most dramatic in the bluest bands. Therefore, we must allow a smooth degradation of S^{optics} as a function of wavelength (estimated as a first-order correction; I have to put the math somewhere in here).

4.3.2 In-situ Measurements of Chromatic Throughput from CBP

The term S^{CBP} describes the in-situ chromatic estimate (with an arbitrary normalization) from the "static" CBP: including the filter (as a function of wavelength and position); the mirrors M1, M2, and M3 (as a function of wavelength); the lenses L1, L2, ?? (as a function of wavelength); and the detector quantum efficience (QE) as a function of position. For Y1 calibrations we assume that $S^{\text{CBP}}(x, y, \lambda)$ is constant for each detector, and will refine this in future versions of the calibration system. Overall, we expect that the CBP measurements should agree with lab data for detector QE and vendor measurements of filter throughput as a function of position. Note that we could use monochromatic flats like the DECal system (ref) to achieve the same in-situ chromatic throughput estimation, although ghosting due to unfocused light makes this much easier with the CBP.

4.3.3 Reference Flux Flats

The term S^{refflux} is the reference flux flat which normalizes the response to focused light (see, e.g. B17). Nominally, this has chromatic variations at small scales (particularly the ITL detectors in the bluest bands), but for Y1 we are assuming any chromatic variations are assumed to be constant at the detector scale and described by the $S^{\text{CBP}}(\lambda)$. Therefore, this term is just the achromatic (gray) portion of the instrumental throughput which can vary from pixel to pixel.

The reference flux flat has a few key differences from the "dome flat" which is obtained by

measuring the response to a Lambertian source of light such as the dome screen. First of all, the dome flat contains a factor of the pixel area $\Omega(x, y)$, which means that it assumes pixel size variations are QE variations. Second, there are differences in focused and scattered light patterns from a flat field screen and distant sky sources. Third, the dome flat is contaminated by scattered light. Finally, the SED of the dome flat does not match the reference spectrum. This final problem we will fix in future data processing by synthesizing broadband flats from narrow-band flats. Nevertheless, we still start with dome flats as they are the most efficient way of measuring the relative response of all the billions of pixels in LSSTCam on small scales.

The dome flat is a good start for estimating the reference flax flat, but has issues at small scales and large scales. At small scales, there are lateral electric field effects such as "tree rings" and the "picture frame" that are pixel size variations that show up as apparent QE variations in the dome flat. At large scales, the response to focused light is different than the dome flat which includes unfocused and scattered light.

To handle lateral electric field effects we fit templates based on our physical knowledge of the detectors. This includes radial templates for tree rings with a fixed center, and square templates around the edge of the detectors. The exact methodology is TBD.

To handle large scale variations for LSST Y1 we use a "star flat" generated from a sequence of multi-band dithered observations of a moderately dense star field. These observations are cross-calibrated using FGCM to generate per-detector polynomial approximations of the throughput relative to the dome flat at scales of hundreds of pixels and greater. By making use of stars of various colors, the FGCM solution can approximate the star flat terms for a flat reference spectrum.

In the future, we plan to use what we call the "dynamic" CBP, where the synthetic stars from the CBP are dithered around the full focal plane. The advantage of this is that the response can be more carefully controlled, and it can be performed in narrow wavelength steps to build up the dynamic CBP star flat with any arbitrary spectrum. The software to perform this analysis will not be ready by the completion of construction.

4.4 Atmosphere Response

The attenuation of light due as it propagates through the atmosphere includes absorption and Rayleigh scattering from molecular constituents (primarily O_2 and O_3); absorption by pre-

ciptable water vapor (PWV), Mie scattering by airborne particulate aerosols that have physical sizes comparable to the wavelength of visible light; and shadowing by ice crystals and water droplets in clouds that is independent of wavelength.

This can be summarized with the following equation:

$$S^{\mathrm{atm}}(\mathrm{alt}, \mathrm{az}, t, \lambda) = S^{\mathrm{molecular}}(\mathrm{bp}, \mathrm{zd}, t, \lambda)\, S^{\mathrm{PWV}}(\mathrm{zd}, t, \lambda)\, e^{-(X(\mathrm{zd})\,\tau(t,\lambda))}, \tag{12}$$

where $S^{\mathrm{molecular}}$ is the absorption and scattering from dry gasses (primarily in the u, g, and r bands); S^{PWV} is the absorption by water vapor (primarily in the z and y bands); τ is the aerosol optical depth (AOD); X is the airmass; and bp is the barometric pressure.

Following FGCM, we obtain the molecular scattering using MODTRAN (ref) combined with the barometric pressure, which is obtained as part of the standard suite of weather data at Cerro Pachon. Ozone absorption can be parameterized by one parameter per night. All constituent throughputs are computed as a function of zenith distance (airmass) in finite steps and interpolated at each wavelength step.

The PWV may vary through the night and as a function of position in the sky. In the FGCM default model the PWV is allowed to vary via a smooth quadratic function through the night. It may also be estimated per visit in the z and y bands by using the relative shift of stars of different colors. As above, we use MODTRAN to determine the absorption as a function of wavelength for a grid of PWV and zenith distance values which are then interpolated.

The aerosol model is a simple Angstrom model with one particular species:

$$\tau(\lambda) = \tau_{7750}\,(\lambda/7750\,\text{Å})^{-\alpha}, \tag{13}$$

where the normalization τ_{7750} and optical index α depnd on the density, size, and shape of the particulates. As with PWV, the AOD normalization is allowed to vary linearly through the night, while the optical index is given a single night.

4.5 Auxiliary Telescope

The Auxiliary Telescope (AuxTel) will be in operation during the LSST survey, obtaining contemporaneous estimates of the atmospheric throughput via low resolution spectroscopy of

bright (sixth magnitude) stars. The mode of operation of AuxTel has not yet been finally determined. We are likely to use different modes in observing when LSST is targeting $ugri$ bands (where more care needs to be taken with the aerosols and ozone) and when LSST is targeting the zy bands (where we need to know the PWV to high precision).

In the first iteration, we plan on using the AuxTel model outputs to validate the FGCM atmospheric model which is determined from the broadband multi-color photometry of the stars observed on a given night. In the future, we may use AuxTel to provide priors on the atmospheric model fit. Considerable care will have to be taken to ensure that outliers from the spectroscopic fits do not contaminate the model used in the broadband photometry. We do not plan to use satellite measurements of atmospheric constituents as priors as the resolution is low enough to be contaminated by observations of neighboring valleys rather than the mountain peak where the telescope is sited.

4.6 Integrating Over Sources

This short section will discuss PSF modeling and aperture photometry and the finit size of stars (and galaxies) and the care that needs to be taken with fluence or surface density images, following B17.

4.7 Foregrounds and Backgrounds

What to do about foregrounds and backgrounds, including fringes? These needs to be written.

4.8 Global Calibration

5 Flat Field System

6 CBP

Flatfield system consists of four main parts: a calibration screen, an aspheric reflector optic, a tunable laser and a white light system.

The calibration screen will be illuminated by either the white light system or a tunable laser.

The white light system will be used for daily flats, while the tunable laser will be used to create monochromatic flats. Both illumination systems are mounted on the dome and co-rotate with the calibration screen. The output of each is co-located at the center of the calibration screen and can be switched between. In order to project that light onto the screen, and additional optic is mounted on the back of the camera and pancake wrap. This is located precisely 3 meters from the projector. It is critical that the projector is aligned with the reflector to ensure a flat illumination pattern on the calibration screen.

6.1 Calibration Screen

The calibration screen is a large reflective surface that can be aligned with the primary mirror and send diffuse light directly to the telescope and camera. It is large enough to illuminate the whole telescope at one time. The surface itself has a diameter of 10.27 meters and an inner diameter of 3.18 meters. Of this area, the section from a diameter of 4.18 - 9.27 meters is coated with a highly reflective material. The outer and inner rings are coated with a very absorptive material. The screen is built of several small panels, with 16 panels making the outer ring and 8 panels making the inner ring. They are secured to a structure such that they are all flat to 3mm across the whole surface. The panels are coated with Labsphere Permaflect 94% and 5% respectively.

The structure on which the panels are mounted can rotate from 0 to -23 degrees relative to horizontal using an actuator. In this way, it can be tilted so that the optical axis of the telescope aligns with teh optical axis of the screen. There will also be 4 retroreflectors mounted around the screen that can be seen by a laser tracker that is mounted on the telescope so that the screen can be easily aligned with the telescope on a daily basis.

Requirements for the screen can be found in LTS-523 and drawings can be found in LTS-126.

6.2 Reflector

The optic that is used to illuminate the calibration screen in full take the shape of an asphere, which is a radially symmetric optic with a radius of curvature that varies radially. The Rubin Observatory aspheric reflector optic was made from a single piece of aluminum, which was

necessary given it's unique shape. The shape of the asphere is given by the following function:

$$Z(s) = \frac{Cs^2}{1 + \sqrt{1 - (1+k)\,C^2 s^2}} + A_4 s^4 + A_6 s^6 + ... \tag{14}$$

where Z is the sage of the surface parallel to the optical axis, s is the radial distance from the optical axis, C is the curvature, k is the conic constant, and A_n are the aspheric coefficients. For this asphere, $C = 1/551.4041743$, $k = -3.92683047$, $A_4 = 0$, and $A_6 = -3.737203 \times 10^{-18}$.

The shape and reflectivity of the optic were measured in the laboratory. The shape was found to match the function within a micron. The reflectivity and scatter from the optic does change across the optic, varying in reflectance from 78 - 82% across the optic.

As mentioned above, the reflector is mounted on the back side of the camera and the pancake wrap. It is mounted on its own hexapod, which can be adjusted manually. When installed, it will be carefully aligned with the optical axis of the telescope, using this hexapod, and then secured in place.

The reflector has a cover which can be opened by command using linear actuators.

6.3 Tunable Laser

The tunable laser is an Ekspla NT242 and capable of producing light from 300 - 2600 nm in 1 nm steps (see fig. 1). It does this by using a combination of a tunable parametric stage using OPO crystals and a sum frequency generation stage. Addiitonally, this laser has a spectral cleaning unit, which slightly reduces the output power but increases the spectral purity by removing some of the primary and secondary harmonics using a prism. The laser interfaces to a Fiber Coupling unit, which makes is easy to switch between outputs, two of which focus the light into fibers. In this way, we can easily switch between sending the light to the flat field or the Collimated Beam Projector.

The laser is designed to operate in room temperature air (18-25°C). It will be housed in an aluminum structure mounted to the dome near the calibration screen and sitting below the CBP. The laser will be kept within this operating temperature range as much as possible using heaters used in a small area (<100W). After use of the laser, heat will be removed from the

enclosure using fans until the enclosure is within 2 degrees of the ambient dome environment. The laser light will be fed into a NA 0.22 optical fiber (Ceramoptic WFNS) and travel ~ 15 m from the laser platform to the CBP and central projector.

The laser can be operated in continuous mode or burst mode. The pulse duration is 3-6 ns, with a repetition rate of 1000 Hz. In continuous mode it will continue to send pulses at this rate. In burst mode, you can select a number of pulses sent in a "burst", after which it will not emit until you tell the laser to send another burst.

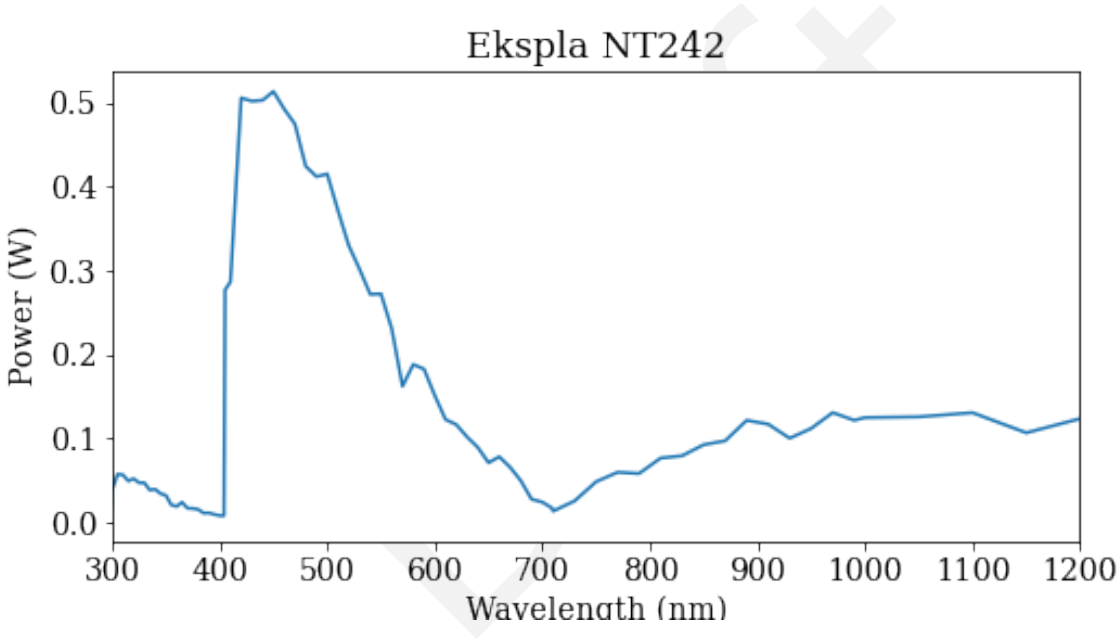

Figure 1: Expected Power output of NT242 Tunable Laser

6.4 White Light System

plot of LEDs Mechanical configuration Optical model Model output

6.5 Projector

6.6 Monitoring systems

We will want to measure precisely how much light from the laser is entering the CBP at a given wavelength so that we determine the exact fraction of that light that is captured by the LSST camera. In order to do that, we need to monitor the luminosity of the laser as it enters the

integrating sphere as well as the spectral properties of the light. This data will be recorded for every measurement made with the CBP in such a way that it can be easily linked to the LSST camera image.

6.6.0.1 Photodiode In order to monitor the exact amount of light injected into the CBP, we use a Hamamatsu S2281 Silicon Photodiode that has been precisely calibrated by NIST. This photodiode, which is mounted directly to the integrating sphere, has a sensitive area of 11 mm in diameter. It is read out by a Keithley 6517b electrometer. The electrometer can measure current, charge, resistance and voltage. Our uses of the CBP will likely use the charge and current modes.

The electrometer can be read out as quickly as every 20 ms. There is a relationship between how long of an exposure you can take and the integration time. At the minimum integration time, you can take an exposure of ~30 seconds. The data is saved in a fits file in the lfa with the elapsed time from the start of the exposure and the value measured. The range can be set to any value from X to Y.

6.6.0.2 Fiber Spectrograph The spectral response of the injected light will be measured by a pair of fiber-fed spectrographs from Avantes SensLine, one for the blue wavelengths (range) and one for the red (range). These spectrographs will actually be housed in the central projection area in the center of the calibration screen. This is where light from the laser can be projected on the calibration screen. The fibers will be situated such that they will measure some fraction of reflected light within the projector box. When we want to measure the spectral response of the light, we will inject the fiber that runs to the calibration screen, take our measurement, and then send the laser light to the CBP. This assumes that the spectral response will not change from one output to another, which we will have to confirm.

The data from the spectrographs will be saved in a fits file in the lfa that will include the wavelength array and the counts measured by the spectrograph at that spacing.

7 CBP

The Rubin CBP was built by DFM Engineering. The design is essentially a Schmidt camera used in reverse. It includes a primary mirror of 33cm diameter, Schmidt Corrector and a 3-element Flat Field Corrector. It produces a beam with an aperture of 24.1 cm and a field of view of 4.1 degrees. The focal length of the CBP is 625mm, and with the LSST focal length at 10.1m, the magnification factor is 16. Therefore, a 100μm pinhole on the CBP would correspond to 1600 μm, or 160 pixels.

Aperture	24.1 cm
Focal Length	62.5 cm
Field of View	4.1 degrees

Table 2: CBP Specifications

The mount of the CBP allows movement in Azimuth and Elevation, with a swing diameter of 51.8”. The locations are controlled by a Galil Digital Motor Controller (DMC) that is mounted on the azimuth housing. It controls the motors, reads the encoders, and interfaces to the control computer over ethernet. Additionally, the DMC controls the focus of the primary mirror and changes and rotates the masks. The azimuth and elevation stages are absolutely encoded with a Renishaw 26-bit on axis encoder.

At the focal plane sits the mask stage, which can hold 5 different masks. The masks can be rotated, driven by worm gears such that all masks are rotated on a common shaft by a single motor. The center mask stage is position encoded using a Renishaw absolute rotary encoder. The mask holder can hold masks with a diameter of 50 mm. Each mask will be laser etched into aluminium and are removable/interchangeable.

The current Integrating Sphere installed on the CBP is a Labsphere 3P-GPS-060-SF. This integrating sphere has an interior diameter of 6 in. (152.4mm) and an exit port of 2.5 in. (63.5 mm), coated with spectraflect coating. In the exit port a photodiode will be mounted and it will be illuminated by an optical fiber. The integrating sphere is held to the mask stage with standoffs. It sits ~ 3 in. from the focal plane/mask. Using `https://www.labsphere.com/wp-content/uploads/2021/09/Integrating-Sphere-Theory-and-Applications.pdf` as a guide to calculate the intensity of light exiting the integrating sphere by multiplying Ls by the flux incident on the integrating sphere.

Major Subsystem Drawing:

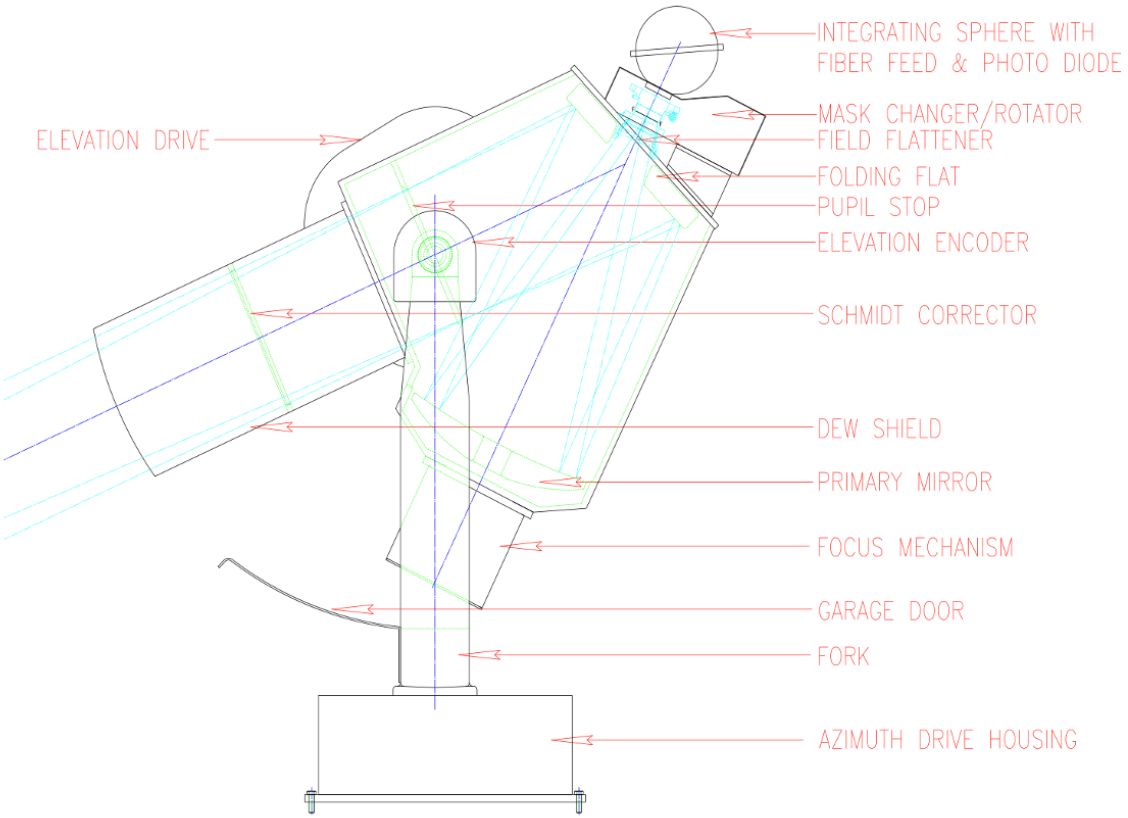

Figure 2: CBP Major subsystems

8 AuxTel/LATISS

9 Camera EOTest Data

10 On-Sky Data

10.1 Twilight Flats

10.2 Dense Dithered Star Fields

11 Plans Post-Year 1

11.1 Synethetic SED matched flats

11.2 Full CBP dataset

Make sure lsst-texmf/bin/generateAcronyms.py is in your path

A Calibration Products List

Quantity	Product Description
Bias	(combined)
Dark	(combined)
CTI	what are these?
PTC	Linearity + Gain
$\mathbf{C}_i$	Crosstalk Matrix
	Defect masks
BF	Brighter-fatter kernels
	Fringe templates (zy)
	Lateral e-field templates
$\mathbf{QE}_{det}$	Sensor QE
$\mathbf{R}_{mirror}$	Mirror reflectivity (Silver x3)
$\mathbf{T}_{filter}$	Filter transmission
	"White" light flats (ugrizy)
T(det, λ)	Transmission
	Dust flat (?)
	Twilight flats (ugrizy; combined)
	Sky flat (combined; ugrizy)
	Reference Flux Flat
	Dense dithered star field + lateral e-field (ugrizy)
	Survey observations

B References

C Acronyms

Acronym	Description

CBP	Collimated Beam Projector
GPS	Global Positioning System
ISR	Instrument Signal Removal
LATISS	LSST Atmospheric Transmission Imager and Slitless Spectrograph
LPM	LSST Project Management (Document Handle)
LSE	LSST Systems Engineering (Document Handle)
LSST	Legacy Survey of Space and Time (formerly Large Synoptic Survey Telescope)
LTS	LSST Telescope and Site (Document Handle)
NIST	National Institute of Standards and Technology (USA)
QE	quantum efficiency
SE	System Engineering
SED	Spectral Energy Distribution
SF	Structure Function
SRD	LSST Science Requirements; LPM-17